Microswimmers Knead Nematics into Cholesterics

Bhavesh Gautam and Juho S. Lintuvuori
Univ. Bordeaux, CNRS, LOMA, UMR 5798, F-33400 Talence, France

(Received 8 January 2024; accepted 30 April 2024; published 3 June 2024)

The hydrodynamic stresses created by active particles can destabilize orientational order present in the system. This is manifested, for example, by the appearance of a bend instability in active nematics or in quasi-two-dimensional living liquid crystals consisting of swimming bacteria in thin nematic films. Using large-scale hydrodynamics simulations, we study a system consisting of spherical microswimmers within a three-dimensional nematic liquid crystal. We observe a spontaneous chiral symmetry breaking, where the uniform nematic state is kneaded into a continuously twisting state, corresponding to a helical director configuration akin to a cholesteric liquid crystal. The transition arises from the hydrodynamic coupling between the liquid crystalline elasticity and the swimmer flow fields, leading to a twist-bend instability of the nematic order. It is observed for both pusher (extensile) and puller (contractile) swimmers. Further, we show that the liquid crystal director and particle trajectories are connected: in the cholesteric state the particle trajectories become helicoidal.

DOI: 10.1103/PhysRevLett.132.238301

Introduction.—Active materials consist of systems where the individual building blocks convert energy into work locally [1]. Examples of this are provided by bacterial fluids [2], catalytic Janus colloids [3], or active microtubules [4] at the micrometer length scale. One of the striking features of these materials is the emergence of collective motion on the scale considerably larger than the particles themselves, such as spontaneous formation of polar flocks in active colloids [5] or the emergence of bacterial turbulence [6]. An interesting subset of active materials is provided by active nematic gels [7]. These consist of active units, force dipoles, with overlaying orientational, nematic order. Pioneering work showed, using linear stability analysis, that the (active) force dipoles can destabilize their nematic order via hydrodynamic instabilities [8–10].

Another example is provided by finite size microswimmers moving in orientationally ordered fluids, where the flow fields created by the swimmers interact with the topology of the surrounding fluid. Typical experimental examples include rodlike bacteria swimming in nematic liquid crystals [11–17]. In the experiments, the bacteria is observed to align along the nematic director [13,17], and the directed motion can be used to, for example, transport cargo [12]. Recent experiments have shown that the liquid crystal (LC) topology can be used to control the swimmers [18–21], such as trapping the particles with topological defects [18] or using LC patterns to create bacterial jets [20], where collective (hydrodynamic) effects play a key role.

The swimming bacteria stir the surrounding fluid which can reorient the nearby nematic. In the simplest case of a uniform nematic LC, experiments in thin, quasi two-dimensional films have demonstrated an orientational instability of the nematic order when bacterial activity is increased [11]. The coupling between the (collective) hydrodynamic effects created by the swimmers and the liquid crystalline elasticity leads to a bend instability of the LC director [11], similarly to what is predicted for extensile active nematic gels [7,8] in two dimensions.

In this work, we open the third dimension and consider microswimmer inclusions in a fully three-dimensional nematic liquid crystal. By using hydrodynamic simulations we study the (collective) dynamics of spherical squirmers in the 3D sample. Our simulations reveal an instability of the uniform nematic order, and a spontaneous formation of a continuous twist is observed. At the steady state, the LC director shows a constant twist along a unique axis, akin to a cholesteric state in passive LCs, and the swimmer trajectories become helicoidal. This spontaneous chiral symmetry breaking arises from the coupling between the swimmer flow fields and the nematic director. There is no prescribed chirality in the system, and indeed, on average, we observe the formation of right- and left-handed helices at approximately equal probabilities. By evaluating the elastic distortions, we show that the spontaneous formation of the continuous twist can be understood in terms of a hydrodynamic twist-bend instability in three dimensions.

Model.—We use a lattice Boltzmann (LB) method to simulate the dynamics of microswimmers in liquid crystals [22,23]. The nematic LC is modeled using a Landau–de Gennes free energy whose density can be expressed as

$$F(Q_{\alpha\beta}) = A_0\left(1-\frac{\gamma}{3}\right)\frac{Q_{\alpha\beta}^2}{2} - \frac{\gamma}{3}Q_{\alpha\beta}Q_{\beta\gamma}Q_{\gamma\alpha} + \frac{\gamma}{4}(Q_{\alpha\beta}^2)^2 + \frac{K}{2}(\partial_\beta Q_{\alpha\beta})^2. \quad (1)$$

The Greek indices denote Cartesian coordinates, and summation over repeated indices is implied. $\mathbf{Q}$ is a symmetric and traceless order parameter tensor, A_0 is a free energy scale, γ is a temperaturelike control parameter giving a order-disorder transition at $\gamma \sim 2.7$, and K is an elastic constant.

The evolution of $\mathbf{Q}$ is given by the hydrodynamic Beris-Edwards equation [24]

$$(\partial_t + u_\nu \partial_\nu) Q_{\alpha\beta} - S_{\alpha\beta} = \Gamma H_{\alpha\beta}, \tag{2}$$

where the first part describes the advection by velocity $\mathbf{u}$ and $S_{\alpha\beta}$ describes the possible rotation or stretching of $\mathbf{Q}$ by the flow [24]. Γ is the rotational diffusion constant, and the molecular field is given by

$$H_{\alpha\beta} = -\delta\mathcal{F}/\delta Q_{\alpha\beta} + (\delta_{\alpha\beta}/3)\mathrm{Tr}(\delta\mathcal{F}/\delta Q_{\alpha\beta}). \tag{3}$$

To simulate the dynamics of the swimmers, we use a squirmer model [25]. The tangential (slip) velocity profile at the particle surface is given by [26]

$$u(\theta) = B_1 \sin(\theta) + \frac{1}{2} B_2 \sin(2\theta), \tag{4}$$

where B_1 and B_2 are constant, giving the strength of the source and force dipoles, respectively, and θ is the polar angle with respect to the particle axis [27]. The source dipole sets the particle swimming speed $u_0 = \frac{2}{3}B_1$, and the ratio $\beta = (B_2/B_1)$ is the squirmer parameter. In the LB method a no-slip boundary condition can be achieved by employing a bounce back on links method [28,29], which needs to be modified for a moving surface [30]. These local rules can include additional terms, such as a surface slip velocity [Eq. (4)] leading to LB simulations of squirming motion [31,32].

The fluid velocity obeys the continuity equation, and the Navier-Stokes equation, which is coupled to the LC via a stress tensor [33]. We employ a 3D lattice Boltzmann algorithm to solve the equations of motion using the Ludwig code [23].

Simulation parameters.—We consider both pushers ($\beta < 0$) and pullers ($\beta > 0$). We fix the $B_1 = 0.0015$, giving the particle velocity $u_0 \equiv \frac{2}{3}B_1 = 10^{-3}$ in lattice units (LU), but vary the force dipole strength B_2 such that $\beta \in [-5, +5]$. We fix the fluid viscosity $\eta = 0.167$ and the swimmer radius $R = 6$ in LU. To model the nematic liquid crystal we use $A_0 = 0.1$, $\gamma = 3.0$, $K = 0.005$, $\xi = 0.7$, $\Gamma = 0.3$, and a rotational viscosity $\gamma_1 = [2(3s/2)^2/\Gamma] = 5/3$, where s is the scalar order parameter of the nematic. The physics of our system is governed by the Reynolds (Re) and Ericksen (Er) numbers, which give the ratio of inertial and viscous forces, as well as the ratio of viscous and elastic forces, respectively. Using the parameters above, we recover $\mathrm{Re} \equiv (u_0 R/\eta) \approx 0.036$ and $\mathrm{Er} \equiv (\gamma_1 u_0 R/K) \approx 2$. All the simulations were carried in a rectangular simulation box $21R \times 21R \times 21R$, with periodic boundary conditions throughout.

Results.—To study the collective dynamics of microswimmers in a three-dimensional nematic liquid crystal, we initialized the system in a uniform nematic state with the $\hat{\mathbf{n}}$ along the x axis [Fig. 1(a)]. The microswimmers were randomly distributed and oriented, while their volume fraction $\phi = [(N4/3\pi R^3)/L_x L_y L_Z]$, and the strength of the force dipole B_2 and thus β were varied. For a low ϕ and a low $|\beta|$ the system remains in a uniform nematic state, and pushers (pullers) have linear trajectories parallel (perpendicular) to the nematic director $\hat{\mathbf{n}}$ [Fig. 1(a)] in agreement with the simulations of isolated swimmers [22]. When the global activity is increased, either by increasing ϕ or the magnitude of β, the uniform nematic becomes

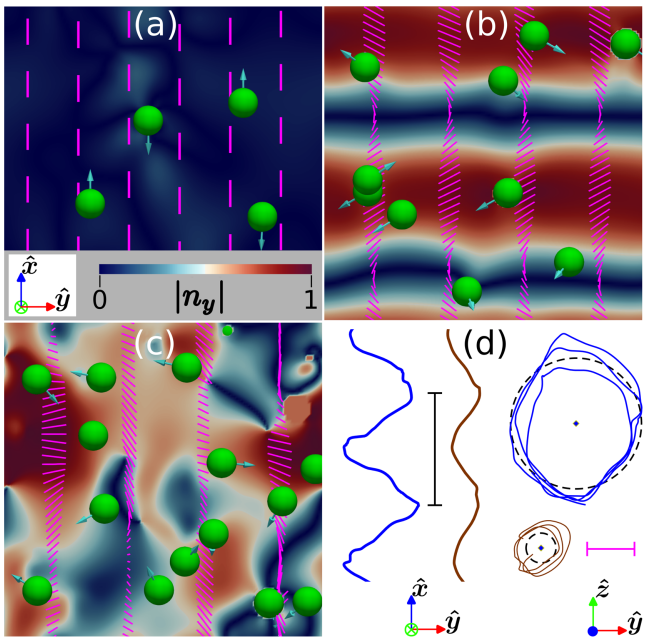

FIG. 1. (a)–(c) Examples of observed states in microswimmer nematic LC composites. (a) At low volume fraction the system is uniform nematic, and pushers (pullers) swim along (perpendicular) to the nematic director $\hat{\mathbf{n}}$. (b) When the activity of the system is increased, the uniform nematic becomes unstable, and a continuously twisting state is observed. The $\hat{\mathbf{n}}$ has a continuous twist along a unique axis (x axis in this case). (c) At high activities, the spatial variations of $\hat{\mathbf{n}}$ become three-dimensional leading to the formation of topological defects. (d) Examples of the unwrapped particle trajectories in the helical state, in the plane along (left) and perpendicular (right) to the helical axis, for pushers (blue lines) and pullers (brown lines), corresponding to $\phi \approx 0.01$ and $\beta = \pm 3.5$, respectively. The dashed lines correspond to a theoretical argument (see text for details). The black scale bar on the left corresponds to the system size $L \approx 21R$, and the pink on the right to $6R$. The data in (a)–(c) correspond to $\beta \approx -2.0$, -2.0, -4.5 and $\phi \approx 0.01$, 0.02, 0.02; the background is color coded according to $|n_y|$, and the nematic director is schematically shown by purple lines.

unstable, and the spontaneous formation of a cholesteric twist is observed [Fig. 1(b)]. At the steady state the $\hat{\mathbf{n}}$ twist continuously around a unique axis, and the particle trajectories become helicoidal [Fig. 1(d)]. Finally, the system loses the cholesteric order at higher activities. The director field variations lack a clear spatial symmetry, and the particle dynamics become chaotic [Fig. 1(c)], as shown in the Supplemental Material [34].

Initially, the nematic director $\hat{\mathbf{n}}$ is along the x axis [Fig. 1(a)]. At the onset of the instability, a continuous twist is observed to develop along this axis. The twist has well-defined handedness and spans the whole system [Fig. 1(b)]. However, there is no inherent chirality in the system. Indeed, in the different ensembles, we observed the formation of both left- and right-handed twists equally (see, e.g., Fig. 3).

At the steady state, the $\hat{\mathbf{n}}$ is well fitted with a helical configuration [Fig. 2(a)]: $n_x = \cos\alpha$, $n_y = \sin\alpha\cos(qx)$, and $n_z = \pm\sin\alpha\sin(qx)$ where $\pm$ corresponds to left- and right-handed twists, α is the tilt angle with respect to the x axis, and q is an inverse pitch length $q = 2\pi/p$. The q is observed to be nearly constant in the helical state for both pushers and pullers, and the pitch length p matches the simulation box length [$p \approx L \approx 21R$; dashed line in Fig. 2(b)]. The tilt angle α is observed to increase upon increasing the strength of the force dipoles, with the tendency being slightly more pronounced for pushers than pullers [open and closed blue circles in Fig. 2(b)].

The particle trajectories and director orientation are connected, and the particle trajectories become helicoidal in the helical state [Fig. 1(d)]. The pitch length of the particle trajectories is approximately given by the pitch length of the LC [Figs. 1(b) and 1(d)]. At the steady, the pushers swim on average along and the pullers perpendicular to the local $\hat{\mathbf{n}}$, leading to a radius of curvature of the helical trajectory $r_t \approx \tan(\alpha)/q$ and $r_t \approx 1/[q\tan(\alpha)]$ for pushers and pullers, respectively. Using the data [$\phi \approx 1\%$ and $\beta \approx \pm 3.5$ in Fig. 2(b)] these give $r_t \approx 7R$ and $r_t \approx 1.6R$ which agree reasonably with the simulations [dashed and solid lines in the right panel of Fig. 1(d)].

In passive achiral nematics, chiral symmetry breaking has been observed to occur due to externally imposed flow and confinement effects [36–44]. Here, the spontaneous formation of the helical states arises from the coupling between the swimmer flow fields and the nematic director $\hat{\mathbf{n}}$. The vorticity ω of the squirmer flow field $\mathbf{v}(\mathbf{r})$ gives rise to a torque on an isolated spherical swimmer in nematic liquid crystals [22]. In living liquid crystal thin films [11,19], a flow instability was shown to arise from the competition between the active (hydrodynamic) torques and elastic aligning torques. We assume a similar mechanism here.

The transition point between the nematic and helical states depends both on the particle volume fraction ϕ and the strength of the force dipole $|B_2|$ (Fig. 3). To phenomenologically relate these quantities to an activity ζ at the continuum limit, we consider the vorticity ω of the squirmer flow field in isotropic fluid $\mathbf{v}(\mathbf{r})$ [45] at a distance r from another swimmer $\omega = \nabla\times\mathbf{v}(\mathbf{r}) = -3/2\sin 2\theta B_2/r^3\hat{\mathbf{e}}_\xi$, where $\hat{\mathbf{e}}_\xi$ is a unit vector along the azimuthal direction. When the density of the particles is uniform, at low ϕ the average distance l between the particles follows $l \sim \phi^{-1/3}$. Using these we can approximate $\zeta \sim B_2\phi$. When all the other material parameters are unchanged, the instability occurs at a (constant) critical value ζ^*. This gives $\phi^* \sim B_2^{-1}$ for the critical volume fraction, which is in agreement with the predictions for

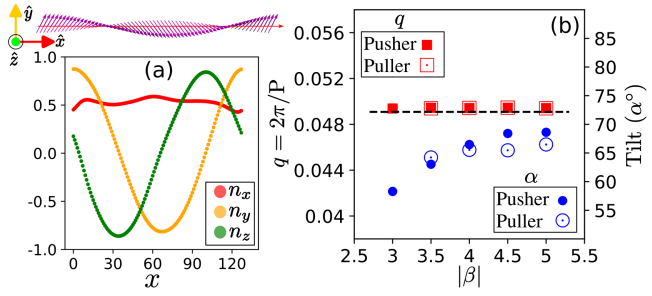

FIG. 2. (a) An example of the LC director components n_x, n_y, and n_z along x axis in the helical state. The data can be fitted by director $\hat{\mathbf{n}}$ corresponding to a cholesteric with x as the helical axis: $n_x = \sin\alpha$, $n_y = \sin\alpha\cos(qx)$, and $n_z = \sin\alpha\sin(qx)$, where α is a tilt angle and $q = 2\pi/p$ is an inverse pitch length. (The data correspond to $\beta = -3.5$ and $\phi = 0.01$). (b) The inverse pitch length q and tilt angle α measured from the simulations as a function of the squirmer parameter β at a volume fraction $\phi \approx 1\%$. The horizontal dashed line marks $q \approx 2\pi/L$, where L is the simulation box length.

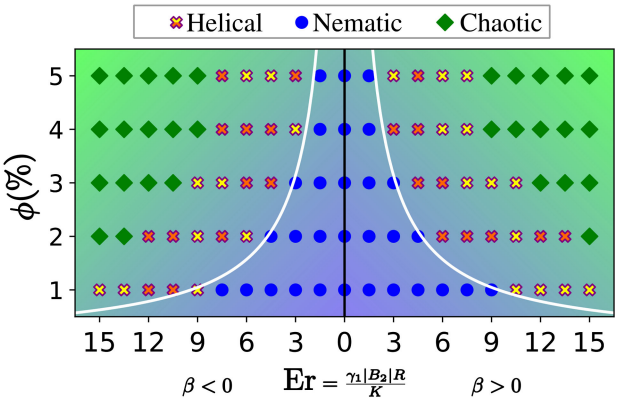

FIG. 3. Steady state phase diagram for the microswimmer-nematic composite material, as a function of the Ericksen number $\mathrm{Er} = [(\gamma_1|B_2|R)/K]$ and the swimmer volume fraction ϕ. The blue spheres correspond to uniform nematic states. The crosses show where the helical states were observed. The purple (yellow) crosses mark the right- (left-) handed helices. The green diamonds correspond to chaotic states. The critical swimmer volume fraction ϕ^* marking the transition between the nematic and helical states is fitted by $\phi^* \sim |B_2|^{-1}$ (see text for details).

confined 2D living liquid crystals [19], and fits the simulation data remarkably well (white lines in Fig. 3). The onset of the helical state is observed to happen at moderate Ericksen numbers and span to low swimmer concentrations $\mathrm{Er} \sim 10$ and $\phi \sim 1\%$, corresponding to experimentally relevant values [11,15].

The system is achiral, and we observe an equal amount of left- and right-handed states (given by yellow and purple crosses in Fig. 3). This suggests that the chiral symmetry breaking arises from an hydrodynamic instability. In two-dimensional extensile active nematics [8] and in thin-film living liquid crystals [11], a bend instability has been observed to be dominant. Our results suggest that the dominant instability is replaced by a twist when the third dimension is opened. Indeed, linear stability analysis has predicted a twist-bend mode to be most unstable in three-dimensional extensile active gels [46,47], and a spontaneous mirror symmetry breaking in the defect dynamics of active nematic gels have been observed both in simulations [48] and in experiments [49]. Very recently a spontaneous flow transition with a well-defined chirality has been predicted in homeotropically confined active nematics [50].

In our system, the equilibrium state of the liquid crystal is a uniform nematic. The swimmer flow fields can perturb this and create (local) deformations, which are penalized by the elastic cost of these distortions. To analyze the different deformations in the system, we calculated the amount of twist, bend, and splay [34,51] across nematic, helical, and chaotic states (Fig. 4). In the nematic state, the system has uniform order, and any deformations are small and localized near the particles (small $|\beta|$ values in Fig. 4). At the onset of the instability, we observe a sudden increase of the distortions. The twist distortions are approximately twice larger than the bend, and 4 times that of splay, for both pushers and pullers (top and bottom panels in Fig. 4, respectively). The chaotic state is marked by the emergence of topological defects [Figs. 4(b) and 4(d)], as shown in the Supplemental Material [34]. The splay distortion is also observed to grow, while the bend and twist deformations remain dominant [large $|\beta|$ values in Figs. 4(b) and 4(d)].

The sudden growth of twist and bend distortions at the transition between the uniform nematic and helical states [Figs. 4(a) and 4(c)], suggests the dominance of the twist-bend mode, in agreement with the linear stability analysis of three-dimensional extensile active nematics [46]. The absence of splay instability for pullers, which has been predicted for contractile active nematics [8], can be understood in terms of the swimming direction of the particles. At the steady state, the pullers swim perpendicular to the (local) nematic director [22]. The perpendicular alignment of an inward (contractile) force dipole with respect to the LC director, corresponds approximately to a parallel alignment of an outward (extensile) force dipole aligned along $\hat{\mathbf{n}}$. Thus the flow instability for both spherical pusher and puller swimmers can be expected to be the same, which agrees with our observations (upper and lower panels in Fig. 4, respectively).

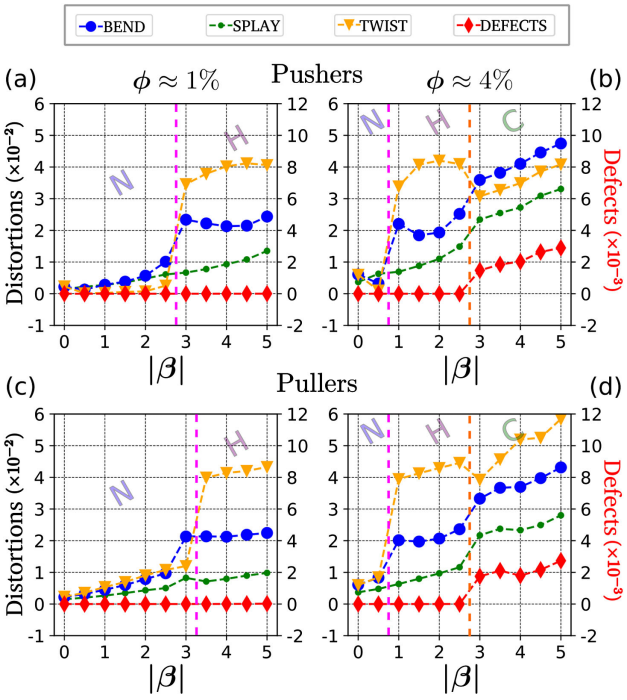

FIG. 4. The bend B (blue circles), splay S (green dots), and twist T (yellow triangles) distortions as well as the defect concentration (red diamonds) measured from the simulations for $\phi \approx 0.01$ and $\phi \approx 0.04$ in the left and right panel, respectively, as a function of the squirmer parameter β. The dashed vertical pink (orange) lines mark the transition between nematic and helical (helical and chaotic) states.

Conclusions.—Using hydrodynamic simulations, we have studied the collective dynamics of microswimmers in nematic liquid crystal. We observe a spontaneous chiral symmetry breaking, where the uniform nematic order becomes unstable and formation of a continuous twist along a unique axis is observed. The particle dynamics follows the LC order, and in the cholesteric state the swimmer trajectories become helical.

There is no inherent chirality in the system. At the steady state, an equal amount of of left- and right-handed helices are observed. The chiral states arise from a hydrodynamic instability, originating from the coupling between the swimmer flow fields and the liquid crystalline elasticity. By evaluating the distortions in the system, we demonstrate that the dominant mode is a twist-bend instability. This agrees with predictions from a linear stability analysis of three-dimensional extensile active nematics [46]. Our predictions could be tested experimentally by opening the third dimension in the experiments of quasi-2D living LCs [11], where the Ericksen number $\mathrm{Er} \sim 10$ and $\phi \sim 0.2\%$, are commensurate with the parameters considered in our simulations. In these experiments, the lateral

size of the system is a lot larger than the predicted periodicity $p \sim 21R \sim 140$ μm, which should allow the helical state to occur. The predictions for pullers could be realized by considering, for example, *Chlamydomonas* which is a near spherical microswimmer with a far-field flow corresponding to a puller force dipole [52].

B. G. and J. S. L. acknowledge the French National Research Agency through Contract No. ANR-19-CE06-0012 and la region Nouvelle Aquitaine project Guiding Artificial Self-Propelling Particles for funding, and cluster Curta for computational time.

[1] S. Ramaswamy, The mechanics and statistics of active matter, Annu. Rev. Condens. Matter Phys. **1**, 323 (2010).
[2] I. S. Aranson, Bacterial active matter, Rep. Prog. Phys. **85**, 076601 (2022).
[3] S. J. Ebbens and D. A. Gregory, Catalytic Janus colloids: Controlling trajectories of chemical microswimmers, Acc. Chem. Res. **51**, 1931 (2018).
[4] T. Sanchez, D. T. Chen, S. J. DeCamp, M. Heymann, and Z. Dogic, Spontaneous motion in hierarchically assembled active matter, Nature (London) **491**, 431 (2012).
[5] A. Bricard, J.-B. Caussin, N. Desreumaux, O. Dauchot, and D. Bartolo, Emergence of macroscopic directed motion in populations of motile colloids, Nature (London) **503**, 95 (2013).
[6] C. Dombrowski, L. Cisneros, S. Chatkaew, R. E. Goldstein, and J. O. Kessler, Self-concentration and large-scale coherence in bacterial dynamics, Phys. Rev. Lett. **93**, 098103 (2004).
[7] A. Doostmohammadi, J. Ignés-Mullol, J. M. Yeomans, and F. Sagués, Active nematics, Nat. Commun. **9**, 3246 (2018).
[8] R. A. Simha and S. Ramaswamy, Hydrodynamic fluctuations and instabilities in ordered suspensions of self-propelled particles, Phys. Rev. Lett. **89**, 058101 (2002).
[9] S. Ramaswamy and M. Rao, Active-filament hydrodynamics: Instabilities, boundary conditions and rheology, New J. Phys. **9**, 423 (2007).
[10] R. Voituriez, J.-F. Joanny, and J. Prost, Spontaneous flow transition in active polar gels, Europhys. Lett. **70**, 404 (2005).
[11] S. Zhou, A. Sokolov, O. D. Lavrentovich, and I. S. Aranson, Living liquid crystals, Proc. Natl. Acad. Sci. U.S.A. **111**, 1265 (2014).
[12] P. C. Mushenheim, R. R. Trivedi, H. H. Tuson, D. B. Weibel, and N. L. Abbott, Dynamic self-assembly of motile bacteria in liquid crystals, Soft Matter **10**, 88 (2014).
[13] I. I. Smalyukh, J. Butler, J. D. Shrout, M. R. Parsek, and G. C. L. Wong, Elasticity-mediated nematiclike bacterial organization in model extracellular DNA matrix, Phys. Rev. E **78**, 030701(R) (2008).
[14] P. C. Mushenheim, R. R. Trivedi, D. B. Weibel, and N. L. Abbott, Using liquid crystals to reveal how mechanical anisotropy changes interfacial behaviors of motile bacteria, Biophys. J. **107**, 255 (2014).
[15] S. Zhou, O. Tovkach, D. Golovaty, A. Sokolov, I. S. Aranson, and O. D. Lavrentovich, Dynamic states of swimming bacteria in a nematic liquid crystal cell with homeotropic alignment, New J. Phys. **19**, 055006 (2017).
[16] H. Chi, M. Potomkin, L. Zhang, L. Berlyand, and I. S. Aranson, Surface anchoring controls orientation of a microswimmer in nematic liquid crystal, Commun. Phys. **3**, 162 (2020).
[17] M. Goral, E. Clement, T. Darnige, T. Lopez-Leon, and A. Lindner, Frustrated 'run and tumble' of swimming *Escherichia coli* bacteria in nematic liquid crystals, Interface Focus **12**, 20220039 (2022).
[18] C. Peng, T. Turiv, Y. Guo, Q.-H. Wei, and O. D. Lavrentovich, Command of active matter by topological defects and patterns, Science **354**, 882 (2016).
[19] M. M. Genkin, A. Sokolov, O. D. Lavrentovich, and I. S. Aranson, Topological defects in a living nematic ensnare swimming bacteria, Phys. Rev. X **7**, 011029 (2017).
[20] T. Turiv, R. Koizumi, K. Thijssen, M. M. Genkin, H. Yu, C. Peng, Q.-H. Wei, J. M. Yeomans, I. S. Aranson, A. Doostmohammadi *et al.*, Polar jets of swimming bacteria condensed by a patterned liquid crystal, Nat. Phys. **16**, 481 (2020).
[21] R. Koizumi, T. Turiv, M. M. Genkin, R. J. Lastowski, H. Yu, I. Chaganava, Q.-H. Wei, I. S. Aranson, and O. D. Lavrentovich, Control of microswimmers by spiral nematic vortices: Transition from individual to collective motion and contraction, expansion, and stable circulation of bacterial swirls, Phys. Rev. Res. **2**, 033060 (2020).
[22] J. S. Lintuvuori, A. Würger, and K. Stratford, Hydrodynamics defines the stable swimming direction of spherical squirmers in a nematic liquid crystal, Phys. Rev. Lett. **119**, 068001 (2017).
[23] Ludwig: A lattice Boltzmann code for complex fluids https://github.com/ludwig-cf/ludwig version 0.20.1.
[24] A. N. Beris and B. J. Edwards, *Thermodynamics of Flowing Systems: With Internal Microstructure* (Oxford University Press, New York, 1994), 36.
[25] M. J. Lighthill, On the squirming motion of nearly spherical deformable bodies through liquids at very small Reynolds numbers, Commun. Pure Appl. Math. **5**, 109 (1952).
[26] V. Magar, T. Goto, and T. J. Pedley, Nutrient uptake by a self-propelled steady squirmer, Q. J. Mech. Appl. Math. **56**, 65 (2003).
[27] K. Ishimoto and E. A. Gaffney, Squirmer dynamics near a boundary, Phys. Rev. E **88**, 062702 (2013).
[28] A. J. C. Ladd, Numerical simulations of particulate suspensions via a discretized Boltzmann equation. Part 1. Theoretical foundation, J. Fluid Mech. **271**, 285 (1994).
[29] A. J. C. Ladd, Numerical simulations of particulate suspensions via a discretized Boltzmann equation. Part 2. Numerical results, J. Fluid Mech. **271**, 311 (1994).
[30] N.-Q. Nguyen and A. J. C. Ladd, Lubrication corrections for lattice-Boltzmann simulations of particle suspensions, Phys. Rev. E **66**, 046708 (2002).
[31] I. Llopis and I. Pagonabarraga, Hydrodynamic interactions in squirmer motion: Swimming with a neighbour and close to a wall, J. Non-Newtonian Fluid Mech. **165**, 946 (2010).
[32] I. Pagonabarraga and I. Llopis, The structure and rheology of sheared model swimmer suspensions, Soft Matter **9**, 7174 (2013).

[33] M. Cates, O. Henrich, D. Marenduzzo, and K. Stratford, Lattice Boltzmann simulations of liquid crystalline fluids: Active gels and blue phases, Soft Matter **5**, 3791 (2009).
[34] See Supplemental Material at http://link.aps.org/supplemental/10.1103/PhysRevLett.132.238301 for the details of the calculation of the twist, bend, and splay deformations as well as the defect density. It also includes two additional figures showing particle trajectories and topological defects in the chaotic state, as well as Ref. [35].
[35] *Soft Matter Physics: An Introduction*, edited by M. Kleman and O. D. Lavrentovich (Springer, New York, 2003).
[36] S. Čopar, Ž. Kos, T. Emeršič, and U. Tkalec, Microfluidic control over topological states in channel-confined nematic flows, Nat. Commun. **11**, 59 (2020).
[37] G. A. Vásquez-Montoya, T. Emeršič, N. Atzin, A. Tavera-Vázquez, A. Mozaffari, R. Zhang, O. Guzmán, A. Snezhko, P. F. Nealey, and J. J. de Pablo, Control of liquid crystals combining surface acoustic waves, nematic flows, and microfluidic confinement, Soft Matter **20**, 397 (2024).
[38] K. Nayani, R. Chang, J. Fu, P. W. Ellis, A. Fernandez-Nieves, J. O. Park, and M. Srinivasarao, Spontaneous emergence of chirality in achiral lyotropic chromonic liquid crystals confined to cylinders, Nat. Commun. **6**, 8067 (2015).
[39] J. Jeong, L. Kang, Z. S. Davidson, P. J. Collings, T. C. Lubensky, and A. Yodh, Chiral structures from achiral liquid crystals in cylindrical capillaries, Proc. Natl. Acad. Sci. U.S.A. **112**, E1837 (2015).
[40] H. Baza, T. Turiv, B.-X. Li, R. Li, B. M. Yavitt, M. Fukuto, and O. D. Lavrentovich, Shear-induced polydomain structures of nematic lyotropic chromonic liquid crystal disodium cromoglycate, Soft Matter **16**, 8565 (2020).
[41] G. Park, S. Čopar, A. Suh, M. Yang, U. Tkalec, and D. K. Yoon, Periodic arrays of chiral domains generated from the self-assembly of micropatterned achiral lyotropic chromonic liquid crystal, ACS Central Sci. **6**, 1964 (2020).
[42] A. Sharma, I. L. H. Ong, and A. Sengupta, Time dependent lyotropic chromonic textures in microfluidic confinements, Crystals **11**, 35 (2020).
[43] Q. Zhang, R. Zhang, B. Ge, Z. Yaqoob, P. T. So, and I. Bischofberger, Structures and topological defects in pressure-driven lyotropic chromonic liquid crystals, Proc. Natl. Acad. Sci. U.S.A. **118**, e2108361118 (2021).
[44] Q. Zhang, W. Wang, S. Zhou, R. Zhang, and I. Bischofberger, Flow-induced periodic chiral structures in an achiral nematic liquid crystal, Nat. Commun. **15**, 7 (2024).
[45] O. S. Pak and E. Lauga, Generalized squirming motion of a sphere, J. Eng. Math. **88**, 1 (2014).
[46] R. Chatterjee, N. Rana, R. A. Simha, P. Perlekar, and S. Ramaswamy, Inertia drives a flocking phase transition in viscous active fluids, Phys. Rev. X **11**, 031063 (2021).
[47] M. R. Nejad and J. M. Yeomans, Active extensile stress promotes 3D director orientations and flows, Phys. Rev. Lett. **128**, 048001 (2022).
[48] T. N. Shendruk, K. Thijssen, J. M. Yeomans, and A. Doostmohammadi, Twist-induced crossover from two-dimensional to three-dimensional turbulence in active nematics, Phys. Rev. E **98**, 010601(R) (2018).
[49] L. C. Head, C. Doré, R. R. Keogh, L. Bonn, G. Negro, D. Marenduzzo, A. Doostmohammadi, K. Thijssen, T. López-León, and T. N. Shendruk, Spontaneous self-constraint in active nematic flows, Nat. Phys. **20**, 492 (2024).
[50] V. J. Pratley, E. Caf, M. Ravnik, and G. P. Alexander, Three-dimensional spontaneous flow transition in a homeotropic active nematic, arXiv:2310.19487.
[51] J. V. Selinger, Interpretation of saddle-splay and the Oseen-Frank free energy in liquid crystals, Liq. Cryst. Rev. **6**, 129 (2018).
[52] K. Drescher, R. E. Goldstein, N. Michel, M. Polin, and I. Tuval, Direct measurement of the flow field around swimming microorganisms, Phys. Rev. Lett. **105**, 168101 (2010).